Peer review status:
This is a non-peer-reviewed preprint submitted to JGR: Solid Earth.

Title:
The 'trench pull' force: constraints from elasto-plastic bending models

Author:
Dan Sandiford

Email:
dsand@unimelb.edu.au

The 'trench pull' force: constraints from elasto-plastic bending models

Dan Sandiford[1]

[1]University of Melbourne

Key Points:

- Trench pull refers to the net force associated with the pressure deficit beneath the trench, relative to an isostatic column in the plate
- The force can be quantified using an extended concept of 'GPE*' which accounts for a pseudo-density (ρ^*)
- Elasto-plastic models are used to constrain the distribution of ρ^* and the magnitude of the trench pull, estimated to be around 2.5 $\mathrm{TN\,m^{-1}}$

Corresponding author: Dan Sandiford, dsand@unimelb.edu.au

Abstract

Stresses transmitted through slabs are thought to provide an important component of the driving force on the trailing plates. This 'net slab pull' is usually conceptualised in terms of in-plane differential stress, acting in the sense of deviatoric tension. However, an additional component of the net slab pull arises due to the pressure deficit created by plate downbending. The purpose of this paper is to investigate the mechanics and typical magnitude of this mechanism, which is termed 'trench pull'. The challenge is that because trench topography is non-isostatic, the pressure distribution cannot be treated with the lithostatic approximation that has been exploited, with much insight, in other settings. Here, the relative pressure reduction depends on the vertical distribution of *horizontal gradients of the vertical shear stress*. These stress gradients are denoted $Q(z)$, and $Q(z)/g$ can be interpreted as a pseudo-density ρ^*. The concept of the force due to gravitational potential energy differences (ΔGPE*) is extended to include the effect of $\rho^*(z)$. In terms of the contribution to the ΔGPE*, the distribution of $\rho^*(z)$ functions exactly like the real density - notably there is the same dependence on the vertical center of mass. In this study, elastic and elasto-plastic models are used to investigate this problem, specifically the distribution of the vertical shear stress and its partial derivatives. A key conclusion is that the length scale over which the trench pressure deficit acts is half the mechanical thickness of the lithosphere. Based on this model, a typical trench pull force is estimated to be about 2.5 $\mathrm{TN\,m^{-1}}$. The total topography that exists between ridges and trenches is associated with a net driving force of about 5 $\mathrm{TN\,m^{-1}}$, enough to balance basal drag of 1 MPa, over a plate length of 5000 km.

1 Introduction

A long-standing goal of geodynamics has been to the understand the force balance associated with the motion of the tectonic plates. This has led to the characterisation and analysis of various distinct contributions (e.g., Lister (1975); Forsyth and Uyeda (1975)). Some of these, such as the difference in integrated pressure due to isostatic subsidence (or ridge push) can be estimated with relatively few assumptions, and the magnitudes are uncontroversial (Lister, 1975; Bird, 1998). Other components are inherently harder to estimate, and rely on inferences based on different combinations of modelling and constraints, with a range of different conclusions resulting. A case in point is the magnitude of the horizontal force that is propagated directly from slabs to the trailing plates (the so-called net slab pull) (Forsyth & Uyeda, 1975; Conrad & Lithgow-Bertelloni, 2002). As previous studies have recognised, stresses propagated through the slab may actually produce two kinds of driving force in the trailing plate (Richter et al., 1977; Bird, 1998; Bird et al., 2008; Bercovici et al., 2015). The standard (textbook) conceptual model emphasises only one of these - where the net slab pull arises due to an in-plane differential stress (i.e. deviatoric tension). An additional component of the net slab pull arises due the topography of the trench, and has been referred to as 'trench pull' (e.g, Bird (1998)). Of the various mechanisms proposed to contribute to the tectonic force balance, trench pull is perhaps one of the least well understood (or recognised). Fundamentally this owes to the challenge of constraining the pressure distribution with depth in the bending plate. The relative pressure reduction depends the vertical distribution of *horizontal gradients of the vertical shear stress*, and is therefore fundamentally linked to the way in which the non-isostatic deflection is supported within the plate. The purpose of this study is to investigate the mechanics, and try to estimate the typical magnitude of this trench pull force.

2 Background

The correlation between plate velocity and attached slab length, corroborated by various types of modelling, underpins the current consensus regarding the importance of slabs in the overall tectonic force balance (Forsyth & Uyeda, 1975; Conrad & Lithgow-Bertelloni, 2002; Saxena et al., 2023). Several modes of slab-plate coupling have been proposed; one widely discussed dichotomy is that of slab pull versus slab suction (Forsyth & Uyeda, 1975; Conrad & Lithgow-Bertelloni, 2002). Suction-type forces, for instance driven by ancient slab masses in the lower mantle, are argued to be important drivers of plate motion (Bird, 1998; Becker & O'Connell, 2001). The current study addresses only the pulling-type mode, which arises due to the slab's capacity to act as a stress guide (Elasasser, 1969).

The stresses that are available to pull directly on the trailing plate, will arise from a residual of the sum of body forces and tractions acting on the slab (Forsyth & Uyeda, 1975; Bird, 1998). The horizontal component of this residual is often referred to as the 'net slab pull'. This force will be expressed in a stress anomaly across a section of the plate at the trench. This residual may also contribute to vertical loads (i.e., a shear stress resultant) and bending moments acting on the trailing plate. These are the loading patterns typically associated with the non-isostatic downbending of the trailing plate (Parsons & Molnar, 1976; Turcotte et al., 1978; Turcotte & Schubert, 2002; Garcia et al., 2019).

Because net slab pull arises from a sum of contributions, many involving significant uncertainty, direct estimation is not possible (c.f. ridge push). Instead, various studies (too many to list in full) have sought to infer the relative influence of net slab pull, using a variety of modelling approaches and constraints on both the global and an individual plate scale (Forsyth & Uyeda, 1975; Bird, 1998; Conrad & Lithgow-Bertelloni, 2002; Copley et al., 2010; England & Molnar, 2022). Net slab pull has also been investigated through direct forward modelling, via analysis of the stress/deformation state in the trailing plate (Schellart, 2004; Capitanio et al., 2010; D. Sandiford & Craig, 2023). The results from various approaches have a significant degree of inconsistency: some studies suggest that the net slab pull is similar (within about a factor of 2) to the estimated ridge push in old lithosphere (Forsyth & Uyeda, 1975; Richardson et al., 1979; M. Sandiford et al., 2005; Schellart, 2004; Bird et al., 2008; Copley et al., 2010; England & Molnar, 2022). Others have argued that (depending on assumptions), net slab pull could be between about 3-4 times larger (e.g., van Summeren et al. (2012); Clennett et al. (2023), to almost an order of magnitude larger (e.g. Conrad and Lithgow-Bertelloni (2002)) than typical ridge push estimates.

Although the magnitude of net slab pull remains debated, the mode of force propagation has typically been less controversial. The prevailing conceptual model is that slabs support an anomalous in-plane differential stress that is transmitted 'through the bend' to the trailing plate (Elasasser, 1969; Isacks & Molnar, 1971; Conrad & Lithgow-Bertelloni, 2002; Schellart, 2004; Capitanio et al., 2009). In describing the state of stress in slabs we find frequent reference to slabs undergoing downdip extension or stretching and sometimes as being under tension (Richter et al., 1977; Richardson et al., 1979; Schellart, 2004; Molnar & Bendick, 2019; Spence, 1987). In this study the term 'in-plane resultant' (symbolised F_D) encapsulates the stress state envisaged in this paradigmatic model. The subscript D is employed to signify differential or deviatoric. Fig. 1 shows a simple example of a stress state giving rise to positive in-plane resultant (i.e., deviatoric tension).

However, as previous studies have recognised, there is additional mechanism that contributes to the net slab pull (Richter et al., 1977; Bird et al., 2008; Bercovici et al., 2015). Bird (1998) refers to this force as 'trench pull', which is the term adopted here. As described in Richter et al. (1977), the force arises due to the topography of trenches:

> A driving force may arise in the same way as that at ridges. Because mantle rock is replaced by water, the lithostatic pressure at all depths is reduced [1] by $(\rho_m -$

[1] for reference, this reduction is about 80 MPa, for a relative trench depth of 3.5 km

> $\rho_w)gH$, where H is the depth of the trench. However, unlike ridges, trenches are not isostatically compensated and must be maintained by elastic forces. Unfortunately, very little is yet known about the distribution of these stresses. It is not even clear whether any of the pressure reduction is available to drive the plates.

Of the various mechanisms proposed to contribute to the tectonic force balance, trench pull is perhaps one of the least well understood. Although the development of a pressure reduction has recognised by previous studies, essential aspects of the mechanics have remained unexplored/undeveloped (Richter et al., 1977; Bird et al., 2008; Bercovici et al., 2015). The primary reason for this, as mentioned in the above quote, relates to the non-isostatic nature of trench topography.

Fundamentally, there are two key questions we would like to know in regard to trench pull: 1) can we constrain the typical magnitude of trench pull force from basic principles/assumptions, in a similar way to ridge push?; and 2) could trench pull represent a significant component of the net slab pull? The first question is the primary issue addressed in the current study. Even if we can resolve this first question, the second question is inevitably tied to the broader debate regarding the magnitude of the net slab pull. As we have we noted, previous studies show significant divergence on this issue. One methodology that has been used to investigate net slab pull is forward subduction modelling (e.g. Schellart (2004)). Recent numerical subduction modelling suggests that trench pull may indeed be the dominant (~ 75 %) component of the net slab pull (D. Sandiford & Craig, 2023). It is not yet known if this is a property of subduction models more generally (including 3D, or global spherical models). However, it is relatively trivial to test this partitioning as part of the retro-analysis of numerical models, as will be discussed in this paper.

In relation to the above quote from Richter et al. (1977), the key conclusions of this study are:

- some of the pressure reduction is available to drive the plates
- pressure is not reduced *at all depths*
- the pressure deficit equilibrates across the mechanical lithosphere, and is controlled by the distribution of horizontal gradients in the vertical shear stress (Q)
- the length scale over which trench pressure deficit acts is half the mechanical thickness of the lithosphere
- the trench pull magnitude is similar to the estimated ridge push for old lithosphere

The organisation of the paper is as follows: Section 2 contains the mathematical framework and general assumptions. The emphasis is to clearly explain the vertically-integrated, horizontal force balance on the lithosphere. Section 3 considers the distribution of vertical shear stress (and its horizontal gradients: Q, or ρ^*) based on an analytic model of elastic plate flexure. The elasto-perfectly plastic case, is also considered. Section 4 combines these results to provide an estimate of the typical trench pull force. Section 5 provides a brief discussion on some of the implications, observations and tests that are relevant to further investigation of the trench pull mechanism.

3 Modelling assumptions and underlying equations

3.1 preliminaries

Throughout this paper, Earth's subduction dynamics will be approximated by considering a 2D, Cartesian domain, assuming plane strain. We therefore refer to the horizontal (x, positive to the right in figures) and vertical (z, positive down), rather than radial and tangential. We use the continuum-mechanics convention of stress being negative in compression (as shown in Fig. 1). Although we have introduced the concept of trench pull as an effect related to pressure deficit (following (Richter et al., 1977; Bercovici et al., 2015)), the mathematical analysis is developed in terms of the mean stress, σ_{I} (i.e. the negative of the pressure, as shown in Fig. 1).

For timescales of interest, the mantle/lithosphere can be treated as being in static equilibrium. For the symmetric Cauchy stress tensor ($\sigma_{i,j}$, where the first index is the normal vector), the static balance of forces and moments is expressed through the stress equilibrium equation:

$$\int_{\Omega} \sigma_{ij} n_j \, dA + \int_{V} \rho g \delta_{i,z} \, dV = 0 \tag{1}$$

Using Gauss' theorem this can be written in the equivalent form:

$$\sigma_{ij,j} + \rho \delta_{i,z} \, g = 0 \tag{2}$$

With the gravitational acceleration assumed constant and vertical, the horizontal component of integrated tractions on any connected subdomain (Ω) must be zero:

$$\int_{\Omega} \sigma_{jx} n_j \, dA = 0 \tag{3}$$

3.2 The vertically-integrated horizontal force balance

The derivation in this section is simply a representation of the fundamental statement of stress equilibrium (Eq. 3) where the domain is chosen to be representative of a section of lithosphere. Fig. 2 shows a hypothetical section of a subducting plate, extending from the trench to an arbitrary seaward location. We make use of 2 coordinate systems. The z system represents vertical distance from a fixed datum that represents the average shape of the earth (e.g. the ellipsoid or geoid). z_I represents the isostatic level of the lithosphere, we can also write: $z_s(x) = z_I + w(x)$, where $w(x)$ is a standard symbol for the non-isostatic deflection. The z' system denotes distances relative to the plate surface. This local system is more appropriate for describing quantities like the mechanical thickness (z'_m), or the thermal thickness (z'_t).

The choice of domain allows for a key simplification: for the first three boundaries, alignment with the coordinate axes means that the only contribution to the traction is the horizontal normal stress (σ_{xx}) in the case of the vertical boundaries, and the shear stress ($\sigma_{zx} = \tau_{zx}$), in the case of the basal boundary. For these boundaries only the sign of the dot product in Eq. 3 is relevant. Denoting the 4 boundaries shown in Fig. 2 as $\Omega_{0,1,2,3}$, Eq. 3 can be expressed as:

$$\begin{aligned} -\int_{\Omega_0} \sigma_{xx}(x_0, z) dz + \int_{\Omega_1} \sigma_{xx}(x_1, z) dz \\ + \int_{\Omega_2} \tau_{zx}(x, z_c) dx - \int_{\Omega_3} \tau_{jx} n_j (x, z_s) ds = 0 \end{aligned} \tag{4}$$

Of the 4 boundaries of the domain in Fig. 2, only the top one (Ω_3) may vary in terms of its angle WRT to the coordinate system. It is useful to make a simple estimate of this contribution. For subducting plates on Earth, the shear stress of the rock-water interface is of course negligible, the Ω_3 term is dominated by the component of mean stress acting in the x direction due to the local slope. The total hydrostatic contribution is given by integrating the hydrostatic stress, from a depth typical of old isostatic lithosphere (e.g, 4 km), to a depth of additional trench bathymetry (e.g., + 3.5 km). The resulting net force, due to pressure acting on the vertical projection of the slope, is about 0.2 $\mathrm{TN\,m^{-1}}$. Based on the conclusions of this study, the hydrostatic term is more then an order of magnitude smaller than the trench pull due to the same total deflection.

We can simplify the analysis by considering the horizontal force balance on the lithosphere and the water column (i.e., combining the green and blue domains in Fig. 2). The vertical boundaries (Ω_0) now represent the domain extending from z_0 to z_c, and stresses on (Ω_3) make no contribution to the horizontal force balance. What this choice does is take the contribution of the pressure acting on the trench slope, and incorporates it as a small (i.e., second order) change in the quantity we will define as the GPE* at the trench. The advantage is twofold: we have less terms to consider and all vertical integrals have a common lower bound.

It is important to note that the idea of a compensation level is fundamentally a statement about lateral pressure equilibration relative to the average shape of the earth (i.e. $z=$ constant), but *not* at the same depth from Earth's surface (z'). Note that the integration depth in Eq. 4 (z_c) represents a distance relative to the fixed system (z). We now choose a more compact notation, where an overbar symbol is used to represent the vertical integral from z_0 to z_c, so that Eq. 4 can be written:

$$\bar{\sigma}_{xx}(x_1) - \bar{\sigma}_{xx}(x_0) + \int_{x_0}^{x_1} \tau_{zx}(x, z_c)dx = 0 \tag{5}$$

$$\text{or,}\quad \Delta\bar{\sigma}_{xx} + \int_{x_0}^{x_1} \tau_{zx}(x, z_c)dx = 0 \tag{6}$$

This equation says that on a rectangular domain aligned with the axes, and with tractions negligible along the surface, the difference in integrated horizontal normal stress, must balance the integrated shear stresses on the base. It is also commonly expressed in the differential form (Fleitout & Froidevaux, 1983). Although Eq. 6 might be regarded as the fundamental statement of the horizontal force balance, it is not particularly informative in terms of understanding contributions to the lithospheric force balance. We now consider an alternative form, first by expanding the normal stress (σ_{xx}) into the deviatoric/isotropic parts ($\tau_{xx}+\sigma_{\mathrm{I}}$), and then expanding the mean stress in terms of vertical stress quantities; $\sigma_{\mathrm{I}} = \sigma_{zz} - \tau_{zz}$. Making theses substitutions in the LHS of Eq. 6 gives:

$$\Delta(\overline{\tau_{xx} - \tau_{zz}}) + \Delta\bar{\sigma}_{zz} + \int_{\Omega_2} \tau_{zx}(x)dx = 0 \tag{7}$$

The first term on LHS of Eq. 7, represents the difference in vertical integral of ($\tau_{xx}-\tau_{zz}$). The term was previously defined as F_D, and represents the the in-plane differential stress resultant. The second term in Eq. 7 reflects the way vertical normal stress distribution impacts the integrated mean stress. In this study, we use the symbol GPE* to represent the negative of quantity $\bar{\sigma}_{zz}$. The reason for the asterisk and sign will be clarified in the following section. The final term in Eq. 7 is the basal shear force, which will be represented by F_B. Over the wavelength of the trench topography F_B is second order; it is retained in the force balance to provide a form that is also relevant for the plate scale. In symbolic form we have:

$$\Delta F_D - \Delta \mathrm{GPE}^* + F_B = 0 \tag{8}$$

A useful property of this representation of the force balance, is that it separates two distinct contributions that perturb the integrated mean stress (or pressure if one prefers).

One of those contributions has already been identified: it arises when the horizontal principal stress is perturbed, which can be written as $\Delta\sigma_{xx}$, relative to an isostatic background state (e.g., Turcotte and Schubert (2002)). As is shown in Fig. 1, we can write the following equivalent quantities: $\Delta\sigma_{xx} = \tau_{xx} + \Delta\sigma_{\mathrm{I}} = (\tau_{xx} - \tau_{zz})$. The vertical integral (resultant) of these quantities is defined as F_D. The left hand term of Eq.8 therefore captures net forces that arises from a perturbation of the integrated horizontal normal stress; in plane strain this consists of an equal perturbation of the mean stress ($\Delta\sigma_{\mathrm{I}}$) and a horizontal deviatoric component (τ_{xx}). A separate contribution to the integrated mean stress arises from the way vertical normal stress is distributed in the lithosphere (GPE*): the net force due to this effect is represented in the second term of Eq. 8. This term captures effects due to both isostatic topographic changes (like ridge push) as well as the non-isostatic topographic effects, including the trench pull force. However, if the ΔGPE* is approximated by assuming a lithostatic vertical normal stress, it does not provide a valid description of the non-isostatic case.

3.3 The vertical force balance, Q and ρ^*

We have derived a form of the horizontal force balance that includes vertical stress terms. In order to estimate the trench pull - the ΔGPE* that exists between the trench and an isostatic column of lithosphere - we need to develop a model for the distribution of vertical normal stress in each column. Expanding Eq. 2 for the z component, yields:

$$\frac{\partial \sigma_{zz}}{\partial z} + \frac{\partial \tau_{xz}}{\partial x} + \rho g = 0 \tag{9}$$

Integration of Eq. 9 from the vertical origin (z_0) to an arbitrary depth (z) yields the distribution of the vertical normal stress, where ζ is a dummy variable:

$$\sigma_{zz}(x,z) = -\int_{z0}^{z} \rho(x,\zeta) g d\zeta - \int_{z0}^{z} \frac{\partial \tau_{xz}}{\partial x}(x,\zeta) d\zeta \tag{10}$$

To compact the notation, we will use $Q(x,z)$ to symbolise the horizontal derivative of the vertical shear stress:

$$Q = \frac{\partial \tau_{xz}}{\partial x} \tag{11}$$

We now define a quantity which we will refer to as pseudo-density (symbolised ρ^*) and given by:

$$\rho^* = \frac{Q}{g} \tag{12}$$

The definition of ρ^* allows us to write:

$$\sigma_{zz}(x,z) = -g \int_{z0}^{z} \left(\rho(x,\zeta) + \rho^*(x,\zeta)\right) d\zeta \tag{13}$$

The primary purpose for introducing ρ^* is that it: 1) makes the magnitudes associated with the non-isostatic support far more intuitive; 2) allows us to take advantage of the existing framework for analysing the forces related to differences in gravitational potential energy (the symbol GPE* is used to reflect the inclusion of ρ^*). Fundamentally however, the concept of ρ^* is a convenience; any appearance of ρ^* in the remainder of the paper can be substituted for the intrinsic quantity *i.e.*, $(\frac{1}{g}\frac{\partial \tau_{xz}}{\partial x})$.

3.4 Flexural Isostasy

A fundamental principal of geodynamics is that beneath the Earth's strong outer layer there exists a region where vertical normal stresses are approximately equal (i.e. an isobaric compensation level). Of course, this hydrostatic approximation neglects the 'dynamic' topography that arises from variation in normal stresses, associated with flow in the mantle. However, trenches are not viewed as being 'dynamic topography' in this sense, and we therefore we make the normal assumption that trench deflection is completely supported due to the presence of a vertical shear stress within the lithosphere (Turcotte & Schubert, 2002). The compensation principle requires that the LHS of Eq. 10 (or 13) is constant for all lithospheric columns extending to the compensation level. Isostatic compensation occurs when the resultant of Q is zero. For all such columns, the weight of material above the compensation level is equal. When Q has a finite resultant, the lithosphere must deflect vertically (w) from its reference level, so that the lithostatic term changes accordingly, leaving the LHS unperturbed.

For a given deflection from the isostatic level, we can approximate the change in the lithostatic term as $-(\rho_m - \rho_w)gw$. This expresses the fact that vertical motion of a column results in the exchange of between material at the compensation level, and the material above the surface of the lithosphere. For flexure of the oceanic lithosphere, this is the exchange of mantle rock with seawater. The sign is due to the fact that for a positive w there is a loss of weight in the column. We therefore have the relationships:

$$\int_{z_0}^{z_c} \frac{\partial \tau_{xz}}{\partial x}(x,z)dz = (\rho_m - \rho_w)gw(x) \tag{14}$$

$$\int_{z_0}^{z_c} \rho^*(x,z)dz = (\rho_m - \rho_w)w(x) \tag{15}$$

Eq. 15 allows us to make a simple estimate of the magnitude of the pseudo-density that is required to support trenches. For this we use the reference parameters shown in Table 1. If ρ^* is assumed to be constant, all the way to a compensation level, we have $\rho^* \approx 80\,\mathrm{kg\,m^{-3}}$. Note that this is the lower bound, where the shear stress gradients are uniformly distributed down to the compensation level. This constant distribution would also violate the free surface boundary conditions. More accurate models are developed on the next section. Note that, in general, ρ^* can be positive or negative. Around the outer rise, where there is non-isostatic uplift, ρ^* would be negative in order to compensate the excess real density in the column.

If we exchange the order of integration and differentiation in Eq. 14, the connection with the vertical force balance as expressed in the thin plate flexure model becomes clear. In thin plate flexure, the integral of the vertical shear stress across the plate, is termed the vertical shear stress resultant, and is usually symbolised V (Turcotte & Schubert, 2002):

$$\frac{\partial}{\partial x}\int_{z_0}^{z_c} \tau_{xz}(x)dz = (\rho_m - \rho_w)gw(x) \tag{16}$$

$$\frac{\partial}{\partial x}V(x) = (\rho_m - \rho_w)gw(x) \tag{17}$$

3.5 Connection between the vertical and horizontal force balance

We can now define an extended concept of the 'GPE*', which is the 'potential energy' that would be associated with the distribution of real and *and* pseudo density:

$$\mathrm{GPE}^*(x) = -\bar{\sigma}_{zz}(x) \tag{18}$$
$$= -\int_{z_0}^{z_c} \sigma_{zz}(x,z)dz \tag{19}$$
$$= g\int_{z_0}^{z_c}\left(\int_{z_0}^{z}\left(\rho(x,\zeta)+\rho^*(x,\zeta)\right)d\zeta\right)dz \tag{20}$$

This can be transformed into a single integral by reversing the order of integration, where the density distribution is weighted by the height above the compensation level ($z_c - z$):

$$\mathrm{GPE}^*(x) = g\int_{z_0}^{z_c}\left(\rho(x,z)+\rho^*(x,z)\right)(z_c - z)dz \tag{21}$$

The quantity $(\rho(x,z)+\rho^*(x,z))$ can be thought of as a 'corrected density'. As detailed in the appendices, the GPE* represents the first moment of the corrected density around the compensation level. The first moment is equivalent to the center of mass of the distribution, weighted by the integrated value. Any distribution of ρ^* (or ρ) that is symmetric around a point, and has the same integrated value, will make the same contribution to the GPE*. This relationship is emphasised in later parts of the paper.

3.6 Reference parameters

The main objective of this paper is to develop an estimate for the magnitude of the trench pull force, or the ΔGPE*) between the lithosphere the trench compared with an isostatic reference column. The final expression (which is presented in Section 4) depends on 2 main parameters: the relative depth of the trench (w_T), and the mechanical thickness of the lithosphere (z'_m). Based on theoretical and empirical constraints, both of these values are positively correlated with the age of the lithosphere (Goetze & Evans, 1979; Grellet & Dubois, 1982). In discussing a typical value for trench pull, our attention will focus on capturing the behaviour of older lithosphere ($>$ 80 Myr). This as similar to the way in which the ridge push force is usually quoted in the range of 2.5-3.5 $\mathrm{TN\,m^{-1}}$, which is an estimate applicable to the subsidence of old lithosphere (Lister, 1975; Turcotte & Schubert, 2002; Coblentz et al., 2015). Global studies of trench bathymetry suggest that relative trench depths for older lithosphere lie in the range of about 2.5 - 5.5 km and exhibit a positive correlation with the age of the subducting plate (Grellet & Dubois, 1982). A value of 3.5 km is chosen as representative for old lithosphere, but clearly there are significant variations around this value (Grellet & Dubois, 1982; Zhang et al., 2014; Lemenkova, 2019).

4 The distribution of vertical shear stress in bending plates

In the previous section we showed that the coupling between the non-isostatic plate deflection (downbending) and the resulting ΔGPE*, depends on the depth distribution of the shear stress gradient (Q, or ρ^*). In this section we discuss solutions for the depth distribution of the vertical shear stress for uniform elastic plates, and consider the case of elasto-plastic flexure.

4.1 Elastic plates

Vertical shear stresses are a fundamental element of the thin plate flexure model. However, in this framework, shear stresses only appear in terms of the resultant quantity (V), e.g., Eq. 17. Analytic solutions that describe the vertical shear stress distribution can be derived through Airy's method (or stress functions). These are detailed

Name and symbol	Explanation	Related equation / reference value
$z(x)$	surface of plate	- [km]
z_I	depth of isostatic lithosphere	- [km]
$w(x)$	deflection relative to z_I	- [km]
w_T	deflection at trench	3.5 [km]
z'_m	mechanical thickness	60 [km]
z'_{np}	neutral plane depth	30 [km]
z'_t	thermal thickness	100 [km]
z_c	compensation level	$z_I + z'_t$ [km]
$\Delta\sigma_{xx}$	in plane differential stress	$\equiv (\tau_{xx} - \tau_{zz})$ [MPa]
F_D	in-plane resultant	$(\overline{\tau_{xx} - \tau_{xx}})$ $[\mathrm{TN\,m^{-1}}]$
$Q(x,z)$	shear stress gradient	$\equiv \frac{\partial \tau_{xz}}{\partial x}$ $[\mathrm{N\,m^{-3}}]$
$\rho^*(x,z)$	pseudo-density	$\frac{Q}{g}$ $[\mathrm{kg\,m^{-3}}]$
GPE*	negative vert. normal stress integral	$-\bar{\sigma}_{zz}$ $[\mathrm{TN\,m^{-1}}]$
g	gravity	9.8 $[\mathrm{m/s^2}]$
ρ_m	mantle density	3300 $[\mathrm{kg\,m^{-3}}]$
ρ_w	water density	1000 $[\mathrm{kg\,m^{-3}}]$

Table 1. Symbols, definitions, reference parameters and standard units used in this paper. Overbars represent vertical integration across the lithosphere.

in continuum mechanics references, where simple loading loading examples are discussed (Goodier & Timoshenko, 1970). We can approach the solution more directly however, with only the usual assumptions for thin plate flexure (plane bending, zero shear stress on the upper and lower edge) and the stress equilibrium equations. In this section the vertical coordinate (z') has its origin at the center of the plate, the orientations are positive down and to the right As outlined in Appendix A, the distribution of vertical shear stress for an elastic plate of thickness h is parabolic:

$$\tau_{xz}(x, z') = \frac{V(x)}{I}\left(\frac{z'^2}{2} - \frac{h^2}{8}\right) \tag{22}$$

where I is the (2D) first moment of the area. Note that in Eq. 22, V represents the shear stress resultant, meaning the expression on the RHS (excluding V) defines a unit parabola:

$$\hat{\varphi}(z') = \frac{1}{I}\left(\frac{z'^2}{2} - \frac{h^2}{8}\right) \tag{23}$$

$$\int_{-\frac{h}{2}}^{\frac{h}{2}} \hat{\varphi}(z')\, dz = 1 \tag{24}$$

Because $\hat{\varphi}$ is independent of x, the horizontal gradient is also parabolic (e.g., Tanimoto (1957)):

$$\frac{\partial \tau_{xz}(x,z')}{\partial x} = Q(x,z') = \hat{\varphi}(z')\frac{dV(x)}{dx} \tag{25}$$
$$= -\hat{\varphi}(z')f(x) \tag{26}$$

where we have used $\frac{dV(x)}{dx} = -f$, i.e., the expression of vertical force balance in terms of the shear stress resultant (see Eq. 17, or Appendix A). Eq. 26 states that for a uniform 2D elastic plate under the given boundary conditions, the vertical shear stress is always parabolic, and that along the plate, the parabola stretches with a gradient that is proportional to the load (f). Extrapolating this to a uniform elastic lithosphere, and taking f to be the isostatic restoring force, we can write:

$$Q(x,z') = \hat{\varphi}(z')(\rho_m - \rho_w)gw(x) \tag{27}$$
$$\rho^*(x,z') = \hat{\varphi}(z')(\rho_m - \rho_w)w(x) \tag{28}$$

where we have used the fact that a positive (downwards) deflection produces a negative (upward) restoring force.

When thin-plate models are applied to subduction zones, the loading pattern typically consists of a combination of end loads (e.g, V_0), end moments (e.g, M_0), as well as a variable normal load due to the isostatic restoring force (Turcotte & Schubert, 2002). However, to visualise the stress distributions in plane bending, a simpler loading pattern is sufficient. Fig. 3 shows a schematic diagram of the deflection of an elastic plate by a uniformly distributed normal force. The right hand boundary is free, the left boundary is clamped. The deflection, as well as the maximum horizontal stress (σ_{xx}^{Max}) and shear stress (τ_{xz}^{Max}) have analytic solutions, as described in the Figure caption. The upper panels of Fig. 4 show the vertical distribution of (normalised) stress quantities at 2 points in the elastic domain (e1, e2). These profiles emphasise the relationships previously developed in this section. Of particular importance is the parabolic distribution of $Q(z')$. This implies an identical shape for $\rho^*(z')$, which reaches its maximum at (and is symmetric around) the plate center.

4.2 Extension to elastic-plastic plates

In the trench region, the subducting plate is expected to undergo comprehensive yielding and approaches moment saturation. This behaviour is predicted from yield stress envelopes (YSEs) (Chapple & Forsyth, 1979; McNutt & Menard, 1982; Craig et al., 2014), and exhibited in numerical models which incorporate similar constitutive models (Bessat et al., 2020; D. Sandiford & Craig, 2023). Yielding has an important impact on the depth distribution of vertical shear stress (and its gradients) as has been highlighted in engineering literature on bending plates (Horne, 1951; Drucker, 1956). To demonstrate, we follow the approach of Horne (1951), and make the ad-hoc assumption that shear stresses in the bending elastic plate are truncated at a prescribed limit, giving rise to the plastic zones shown in grey in Fig. 3, and the truncated horizontal stress profiles shown on the lower left panel of Fig. 4.

To appreciate the impact on the vertical shear stress, consider the statement of horizontal stress equilibrium (Eq. 2) expanded in the horizontal coordinate:

$$\frac{\partial \sigma_{xx}}{\partial x} + \frac{\partial \tau_{zx}}{\partial z} = 0 \tag{29}$$

Yielding implies that the horizontal gradient of the horizontal stress is zero, which by Eq. 29, implies the vertical gradient of the *horizontal* shear stress is zero, i.e:

$$\frac{\partial \sigma_{xx}}{\partial x} = 0 \implies \frac{\partial \tau_{zx}}{dz} = 0 \tag{30}$$

The boundary condition on the shear stress is assumed to be zero, and so the *horizontal* shear stress must be zero throughout the plastic regions; by symmetry so is the vertical shear stress. In the interior of the elastic core region, the vertical shear stress will remain parabolic, as long as the horizontal stress distribution is linear. In the yielding region, horizontal gradients in vertical shear shear stress (Q) will now depend on the rate at which the elastic core is narrowing, as well as gradient in the shear stress resultant $\frac{dV}{dx}$ (or the normal force). Solutions to this type of problem require non-linear approaches (Turcotte et al., 1978). For the distribution of vertical shear stress shown in Fig. 4, in the limit $\Delta x \to 0$, $Q(z')$ takes the form of truncated parabolas, as shown in the lower right panel. In the limit of the elastic core becoming very thin, $\rho^*(z')$ becomes very large, acting like a point force concentrated at the plate center. For the remainder of the manuscript, an important observation is that that the center of mass of $Q(z')$, (or $\rho^*(z')$) does not change with progressive yielding. Note that if an elasto-plastic plate begins to unbend, vertical shear stress gradients (finite Q) may re-appear where previously they were constrained (by yielding) to be zero. This may be relevant, as models of plate bending often predict that the maximum bending moment occurs slightly seaward of the trench (Turcotte et al., 1978; D. Sandiford & Craig, 2023).

5 Estimating the trench pull force

The trench pull force represents the ΔGPE* between the trench and a isostatic reference column. When it comes to expressing the *difference* in GPE*, based on Eq. 21, we can write:

$$\Delta \text{GPE}^* = -\Delta \bar{\sigma}_{zz} \tag{31}$$

$$= g \int_{z_0}^{z_c} \left(\Delta\rho(z) + \Delta\rho^*(z)\right)(z_c - z)dz \tag{32}$$

which says that the ΔGPE* is an integral function of the difference in the real and psuedo densities. In this expression $\Delta\rho(z)$ means the density of the isostatic column minus the density of the deflected column; this assumes that $\rho(z)$ and $\rho^*(z)$ for both columns are defined on the same fixed vertical coordinate (z).

5.1 Further assumptions

To make use of the models in the previous section, we need to make a choice about the thickness of the lithosphere that supports the relevant stresses (i.e., the thickness to adopt for h). There are various lithospheric length scales that may be relevant, for instance, the thermal thickness (z'_t), the mechanical thickness (z'_m) and the effective elastic thickness (z'_e). In general, ($z'_t > z'_m > z'_e$) (McAdoo et al., 1978). See Table 1 for reference values. The assumption made in the remainder of this paper is that $z'_m (\approx 2z'_{np})$ is the relevant quantity. This assumption is fundamentally tied to how the distribution of vertical shear stress behaves during elasto-plastic yielding. In the monotonic bending of simple uniform plates (Section 3), the distribution of ρ^* has a vertical center of mass given by the depth of the neutral-axis of the plate (z'_{np}). Crucially, this length scale does not change with the onset of yielding. In contrast, z'_e represents an effective quantity - the thickness of an uniform, non-yielding, elastic plate that would support a given bending moment and a given curvature (McNutt & Menard, 1982). For a elasto-plastic plate, the inferred value of z'_e will always be smaller as the curvature grows larger. The is contrary to the way in which the spatial distribution of flexural stresses behaves during progressive bending.

Both observational and modelling constraints suggest the depth interval that contributes to the flexural characteristics of the lithosphere (z'_m) is substantially less than the thermal thickness (Chapple & Forsyth, 1979; Goetze & Evans, 1979). Deeper parts of the lithosphere are effectively irrelevant in terms of the bending moment, and likewise in controlling the depth of neutral plane. While z'_m is not necessarily directly observable, seismological observations show that the 'apparent' neutral plane depth of about 30 - 35 km (Chapple & Forsyth, 1979; Craig et al., 2014). Moreover, there is broad agreement between seismological observations, the neutral-plane depth predicted from laboratory-derived strength envelopes, and the deflection characteristics under these types of strength models. This provides confidence that concept of $z'_m(\approx 2z'_{np})$ is meaningful and reasonably well constrained (Chapple & Forsyth, 1979; Goetze & Evans, 1979; McNutt & Menard, 1982; Craig et al., 2014; Garcia et al., 2019).

A further assumption we make is that ρ^* is zero in the isostatic column. Strictly speaking, isostatic equilibrium requires that only the vertical integral of ρ^* is zero. In principal, a non-zero vertical distribution of ρ^* may exist in the isostatic column, while still exhibiting zero resultant. This assumption means that in order to define $\Delta\rho^*$ we need only to know the vertical distribution of ρ^* in the deflected column.

5.2 Expression/estimate for the trench pull force

The ΔGPE* equation (Eq. 32) is a function of the difference in the distributions of the real and pseudo density, between the isostatic reference column and the deflected column. Due to the assumptions we have introduced (such as neglecting the crust, and assuming ρ^* is zero in the isostatic column) we are left with only 2, non-overlapping contributions to the total (corrected) density differences. The first contribution (to $\Delta\rho(z)$) comes from the real density difference between rock and water. This difference occurs in the vertical section between the isostatic level (z_I) and deflected level ($z_I + w(x)$). The second contribution (given by $\Delta\rho^*(z)$) is due to the presence of vertical shear stress gradients in the deflected column. These are non-zero only between $z_I{+}w(x)$ and $z_I{+}w(x) + z'_m$ (i.e., across the mechanical thickness of the deflected plate).

The depth distribution for three different models of $\Delta\rho^*$ is shown in the left panel of Fig. 5. Two of these models are physically motivated, corresponding the elastic and elasto-plastic distributions of ρ^* (for an arbitrary degree of yielding). The third distribution, which represents constant ρ^*, is shown with the solid black line. The model of constant ρ^* is not not physically consistent, as it doesn't satisfy the boundary conditions or the equilibrium equations. However, because each of the distributions have the same integrated value, and same center of mass, the contribution to the GPE* is identical. The ΔGPE* is the area under the $\Delta\sigma_{zz}$ curves. The model of constant $\rho^*(z)$ is useful, as it leads to a ΔGPE* integral that can be calculated by inspection. This is represented by the area shown in the 2 grey triangles in the middle panel of Fig. 5. The magnitude of the trench pull force is therefore:

$$
\begin{aligned}
\Delta\mathrm{GPE}^* &= (\rho_m - \rho_w) g w_T \left(\frac{w_T + z'_m}{2}\right) && (33)\\
&\approx (\rho_m - \rho_w) g w_T \left(\frac{z'_m}{2}\right) && (34)\\
&\approx (\rho_m - \rho_w) g w_T z'_{np} && (35)
\end{aligned}
$$

For the reference parameters (Table 1), the trench pull force is close to 2.5 $\mathrm{TN\,m^{-1}}$. Based on the way we have set up the problem (as discussed in Section 2.2), this estimate represents the ΔGPE* of the lithosphere and water column. For a lithosphere-only force balance, the ΔGPE* would increase by about 0.2 $\mathrm{TN\,m^{-1}}$, and an additional (equal and opposite) term would appear, representing the effect of the hydrostatic pressure acting on the trench slope.

The red lines in Fig. 5 show the lithostatic approximation, where the distribution of Q (or ρ^*) is neglected in the deflected column. In this case the vertical normal stress does not equilibrate, and the ΔGPE* does not converge with depth. The value is meaningless, as it does not represent the state of stress with depth.

As shown in Appendix B, another way to define the length scale that appears in Eq. 33 is as a difference in the center of mass of $\Delta\rho(z)$ versus $\Delta\rho^*(z)$, weighted by the total mass anomaly (M) due to the deflection:

$$\Delta \mathrm{GPE}^* = M g \Delta z_{\mathrm{cm}} \tag{36}$$

$$= (\rho_m - \rho_w) g w_T \Delta z_{\mathrm{cm}} \tag{37}$$

Because M, as well as the center of mass of $\Delta\rho$ are fixed, the GPE* problem is completely determined by the center of mass of the pseudo-density: The deeper this resides in the lithosphere, the greater Δz_{cm}, the larger the ΔGPE (for a given deflection).

6 Discussion

Several previous studies have discussed the existence of a pressure deficit due to downbending and a resulting driving force (Richter et al., 1977; Bird et al., 2008; Bercovici et al., 2015). To the best of my knowledge, this study represents the first attempt to constrain the typical magnitude of the trench pull force via mechanical analysis of the bending plate. It is notable that the estimated value is similar to that predicted for the ridge push force (i.e, 2.5-3.5 $\mathrm{TN\,m^{-1}}$ for older lithosphere). The implication is that the topography associated with zones of divergence and convergence contributes similar amounts of net driving force the boundary layer (e.g, Hager and O'Connell (1981); Bercovici et al. (2015)).

The estimates presented in this study suggest that the total ΔGPE*, between ridges and trenches, will typically be around 5 $\mathrm{TN\,m^{-1}}$. Is this enough to drive the plates? Assuming shear stresses beneath the oceanic lithosphere are 1 MPa, the estimated ΔGPE* is enough to balance the basal drag force on a plate of about 5000 km, a fairly typical length scale for Earth's subducting plates. There are many studies that infer basal shear stress of significantly less than this, in the range of 0.2-0.5 MPa (Lister, 1975; Melosh, 1977; Richter et al., 1977; Wiens & Stein, 1985; Chen et al., 2021). On the other hand, trench and ridge systems do not sum perfectly constructively on Earth. For the Pacific plate in the Cenozoic, there is about 50 % constructive contribution to the tangential component of the torque, based on trench geometry (D. Sandiford et al., 2024). For idealised plate geometries, however, the total ΔGPE* is sufficient to balance a resisting basal drag, within the uncertainties associated with the latter.

In developing a model for the depth distribution of the relevant stress quantities (i.e. $Q(z)$, or $\rho^*(z)$) various assumptions and simplifications have been made. For instance, we have adopted the standard 'thin plate' assumptions, including a shear stress-free basal boundary, and neglecting plate rotation due to deflection. Likewise, the analysis has assumed uniform constitutive properties. These choices all preserve complete symmetry in the resulting stress distributions (e.g., Fig. 4). Some of these assumptions could be removed with a more sophisticated analytic treatment. Comparison with numerical models is also informative.

D. Sandiford and Craig (2023) analysed the force balance in a 2D finite element subduction model, comprising a 5000 km subducting plate, where flow was completely driven by the imposed density structure (D. Sandiford & Craig, 2023). Analysis showed that F_D was weakly positive (extensional) at the trench, (0.6 $\mathrm{TN\,m^{-1}}$) and that the ΔGPE* - defined relative to the isostatic lithosphere - was about 2.0 $\mathrm{TN\,m^{-1}}$. Therefore, trench pull represented the dominant ($\approx$ 75 %) component of the net-slab pull. The ΔGPE* reported in D. Sandiford and Craig (2023) is also about 75 % of the 'typical' value derived in this study. This suggests that, although based on numerous simplifying assumptions, the expression developed in this study is applicable to the dynamics of more realistic, and complex, bending scenarios.

Bessat et al. (2020) also estimate the 'GPE' variation around the trench, based on retro-analysis of a numerical subduction model. They use the lithostatic stress to approximate the vertical normal stress (hence theirs is an estimate of GPE, not GPE*). The GPE variation due to the trench topography was estimated to be $>$ 50 $\mathrm{TN\,m^{-1}}$. The very large ($\sim 20\times$) discrepancy between this value, versus the current study, is attributable to two factors in their analysis: 1) the lithostatic approximation was used for σ_{zz}; and 2) the vertical integration was extended to the base of the model domain (660 km). Note that, as shown in Fig.5, the lithostatic approximation means the $\Delta\sigma_{zz}$ does not equilibrate with depth. As a result, the ΔGPE* does not converge. Hence, factor 2 is likely to vastly exacerbate factor 1. It is speculated that, had the true vertical normal stress from the numerical model been used, values compatible with Eq. 33 would have been obtained.

It should be relatively straightforward to test generality of these ideas by others in the subduction modelling community. As far as 2D numerical subduction models is concerned, the simplest way to approach an analysis of the trench pull (and its relative role in the net slab pull) is to calculate the variation of F_D seaward the trench. Functionally, this requires approximating the integral of the deviatoric stress difference down to a fixed compensation level (i.e., the first term in Eq. 7). The change in F_D between the trench and the point where the plate returns to the isostatic level ($\sim$ 100 km) is a proxy for the ΔGPE* (the trench pull). This assumes that the basal shear force (F_B)is insignificant over the same horizontal lengthscale. It then remains to assess how the value of ΔF_D compares to F_D evaluated at the trench. If F_D at the trench is positive, and larger than ΔF_D, then it might be reasonable to assume the net slab pull dominated by an in-plane resultant transmitted through the slab hinge (i.e., the textbook mode of slab pull). However, if the ΔF_D is the larger term, then trench pull provides the dominate component of the net slab pull. Note that the dynamics should be very similar even if the surface boundary condition has a 'free slip' type condition. In this case, although there is no deflection, a (roughly equivalent) pressure anomaly will be present; it is through this, that the trench pull force will arise.

In this study, analysis of the trench pull force is developed in terms of the relative trench depth. This is a valid way of framing the problem, as the deflection can be viewed as the 'cause' of the pressure deficit (e.g., Richter et al. (1977)). However, downbending of the subducting plate is typically linked to the presence of a vertical shear stress and/or bending moment acting on a plane beneath the trench. This means that we could also develop a relationship between the trench pull force, and some combination of these loading patterns. Davies (1983) proposed that the net slab pull is approximately equal to the vertical shear stress resultant at the trench (V_0). If we adopt the same assumptions as that study, a uniform elastic plate, and neglecting the bending moment, then V_0 is a linear function of the trench deflection (e.g., Turcotte and Schubert (2002)):

$$V_0 = g(\rho_m - \rho_w) w_T \frac{\alpha}{2} \tag{38}$$

where α is the flexural parameter. Comparison with Eq. 34 shows that V_0 will be equal to the trench pull (ΔGPE*), provided that $\alpha \sim z'_m$. Previous investigations suggest these length scales are indeed comparable (e.g., Caldwell et al. (1976); Goetze and Evans (1979); Hunter and Watts (2016)). Hence, the current study provides support for the relationship proposed by Davies (1983): in simple terms the vertical force due to the slab 'pulling down' on the trailing plate may be roughly equivalent to the horizontal force induced by the resulting pressure deficit (i.e., the trench pull force). However, additional coupling will occur due to the presence of a bending moment.

7 Conclusions

The purpose of this paper has been to investigate the mechanics and typical magnitude of the trench pull force. The description of a net horizontal force due to gravitational potential energy differences (ΔGPE*) is extended to include the effect of a pseudo-density, $\rho^*(z)$, which supports the non-isostatic topography. Elastic and elasto-plastic models are used to investigate this problem, specifically the distribution of $Q(z)$ (or $\rho^*(z)$). A key conclusion is that the length scale over which trench pressure deficit acts is $\frac{z'_m}{2} \approx z'_{np}$. It is shown that this length scale represents the difference in the center of mass of the real density difference ($\Delta\rho$), versus the pseudo density difference ($\Delta\rho^*$). The resulting estimate for a typical trench pull force is about 2.5 $\mathrm{TN\,m^{-1}}$, similar to that associated with isostatic cooling of old lithosphere. The topography that exists between ridges and the trenches ($\approx$ 5-6 km) is likely to be associated with a net force of at least 5 $\mathrm{TN\,m^{-1}}$, enough to balance basal drag of 1 MPa, over a plate length of 5000 km. Comparison between the expression developed in this study, and results based on retro-analysis of numerical model, agree to about 75 %. Others in the subduction modelling community are encouraged to test the generality of these relationships, which are relatively easy to ascertain.

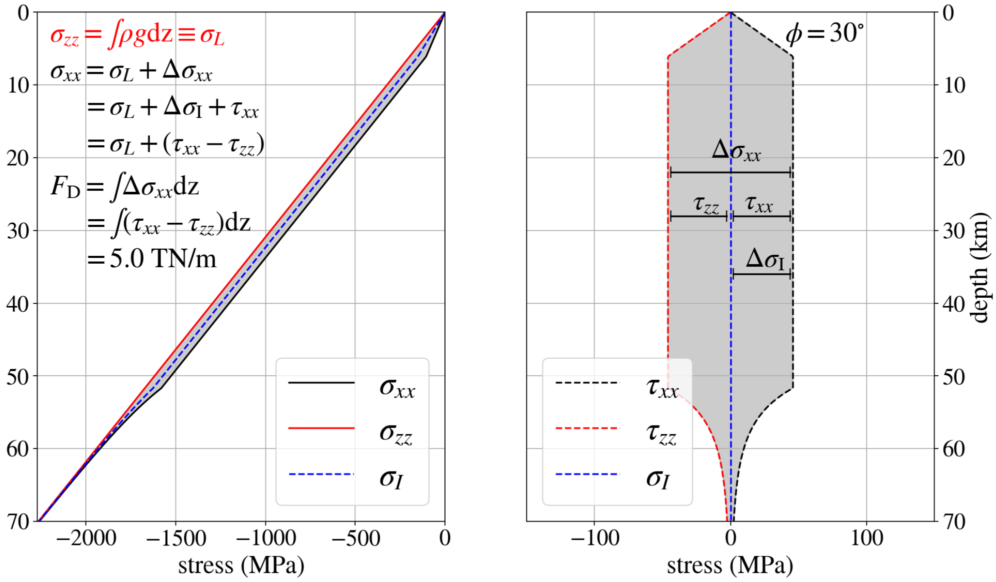

Figure 1. Horizontal and vertical stresses on a hypothetical section across the lithosphere. Compressive stresses are negative. The vertical normal stress (σ_{xx}) is a principal stress, and is assumed to be lithostatic (σ_L). The horizontal normal stress is given by the lithostatic stress, and an additional (differential) stress, symbolised $\Delta\sigma_{xx}$ (e.g., Turcotte and Schubert (2002)). The integral of the differential stress is referred to as the 'in-plane resultant', symbolised F_D. Positive F_D means the horizontal stress is (on average) less compressive than the vertical, i.e, an Andersonian extensional regime, or deviatoric tension. The magnitude of F_D shown in the figure is 5 $\mathrm{TN\,m^{-1}}$. In plane strain, the differential stress can be written in several equivalent ways; $\Delta\sigma_{xx} = (\tau_{xx} - \tau_{zz})$, is an important relationship that will appear in later analysis. The strength model includes frictional behaviour as well as power law creep (Hirth & Kohlstedt, 2003).

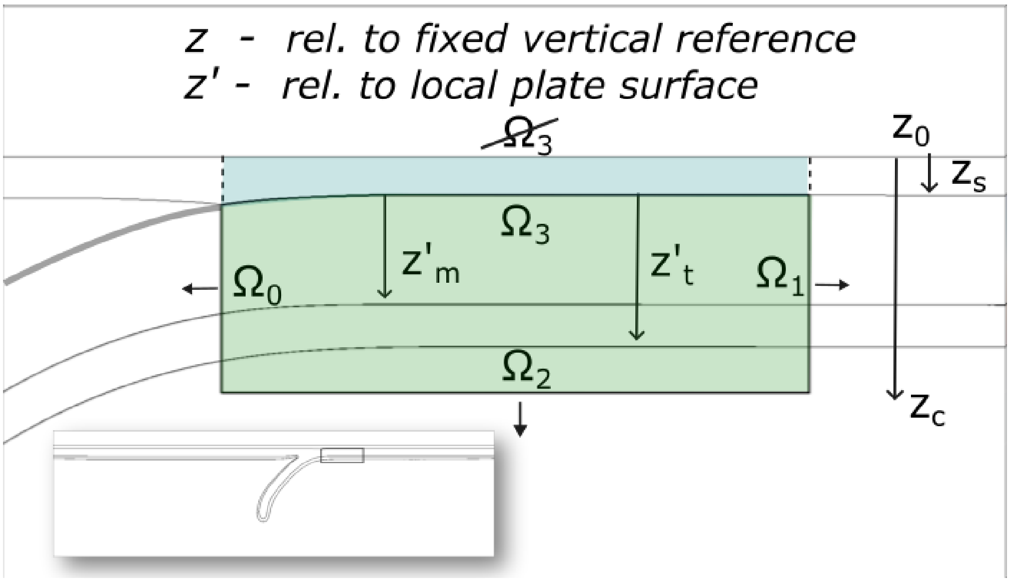

Figure 2. Schematic of a subducting plate, and a subdomain on which the 'vertically integrated' horizontal force balance equations are developed. The green domain represents rock, the blue domain the water column. To simplfy the analysis, we combine the domains, so that Ω_3 moves to the sea surface (at z_0), but makes no contribution to the horizontal force balance. The vertical boundaries ($\Omega_{0,1}$) extend from z_0 to z_c. z'_m represents the mechanical thickness of the lithosphere, typically significantly less than the thermal thickness z'_t. The compensation level is represented by z_c. At this level, vertical normal stresses are approximately equal (exactly equal in the hydrostatic approximation). Here, z_c is taken as a fixed (z = constant) depth equivalent to the lithospheric thermal thickness, i.e, $z_c = z_I + z'_t$. In fact however, based on the models developed in this study, vertical normal stresses always equilibrate at (or above) the base of the mechanical lithosphere. This makes the choice of z_c irrelevant as long as it equal or greater than $z_I + z'_m$. In other words, beneath the depth $z_I + z'_m$, there is no contribution to the net horizontal force arising from the vertical integrals.

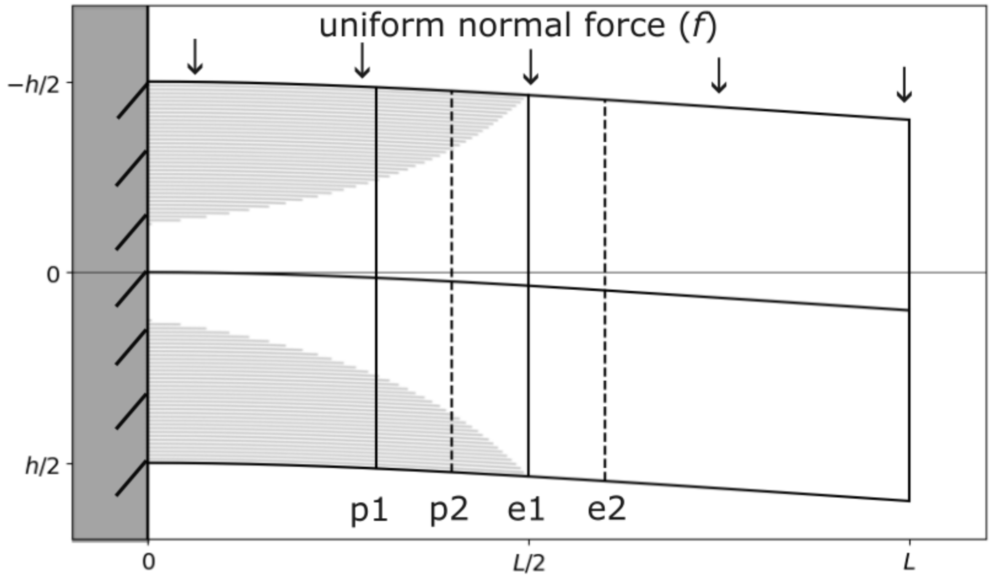

Figure 3. Deflection of a cantilever subject to uniform normal force. The dimensional deflection is: $w(x) = \frac{fx^2}{24EI}\left(6L^2 - 4Lx + x^2\right)$, where f is the normal force. In this figure, f and L are taken as 1, the aspect ratio is 2, and E is chosen to provide a dimensionless deflection $w' = \frac{w}{L}$ of 5%. The general behavior can be represented by scaling stresses by the maximum values: for the horizontal normal stress, $\sigma_{xx}^{Max} = \frac{6fL^2}{h^2}$, and for the shear stresses, $\tau_{xz}^{Max} = \frac{3fL}{2h}$. This is how the stresses along profiles (p1, p2, e1, e2) are represented in Fig. 4. The light grey region shows the zone where yielding is assumed, with the yield limit given by $\tau_{\mathrm{Max}} <= \frac{1}{2}\sigma_{xx}^{Max}$.

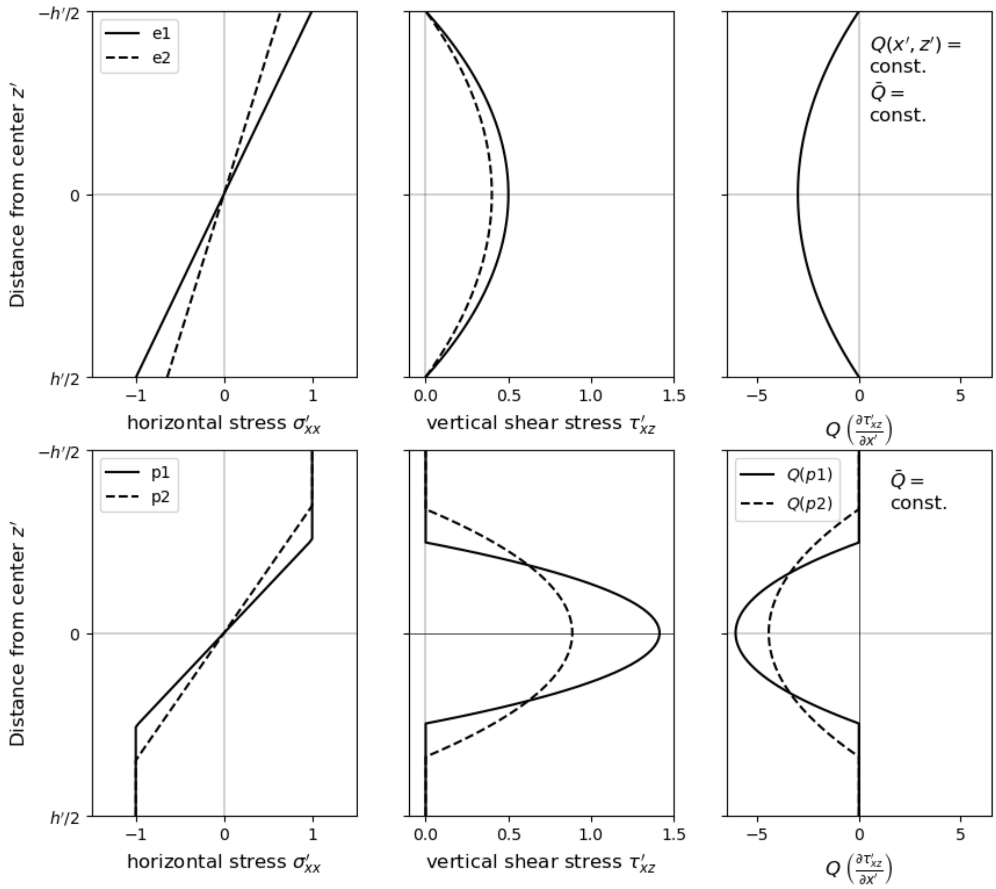

Figure 4. Distribution of stresses in elastic (upper panels), and elasto-plastic (lower panels) domains, after Horne (1951). Normal stresses are scaled using the prescribed value of the yield stress $\sigma_y = \frac{1}{4}\sigma_{xx}^{Max}$; shear stresses are scaled using $0.5\tau_{xz}^{Max}$, as discussed in the Fig. 3 caption. Lengths have been scaled using L. In terms of how the vertical distribution of stress impacts the GPE*, the key quantity is the one shown in the right hand panels - the horizontal gradient of the vertical shear stress. In this paper, we symbolise these gradients Q; we also define $\rho^* = \frac{Q}{g}$. This setup assumes uniform loading, and hence the vertical shear stress resultant ($\bar{Q} \equiv \frac{dV}{dx}$) is constant. In the elastic domain, $Q(x', z')$ is constant everywhere, as shown in the top right hand panel. In the yielding case, $Q(x', z')$ may vary, but the resultant ($\bar{Q}$) remains constant. For the yielding domain, $Q(z) = 0$ in the outer yielding region, and remains parabolic in the inner elastic core region.

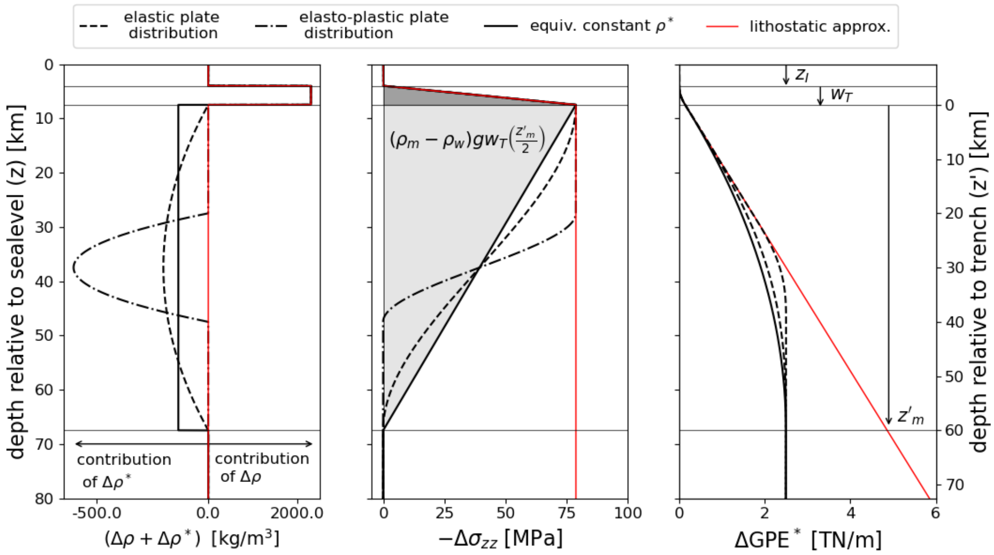

Figure 5. Each panel represents the differences in quantities between the isostatic reference column and a column beneath the trench. The figure uses reference values shown in Table 1. The left hand panel shows the difference in the corrected density between the columns. This represents, the sum of, respectively, the difference in the real density ($\Delta\rho$) and the pseudo density ($\Delta\rho^*$). The vertical integral of this quantity must be zero in order for equilibration of the vertical normal stress to occur (from Eq. 13). The first moment of this quantity, around the compensation level, gives the ΔGPE* (from Eq. 32). The middle panel shows the (negative of) the difference in vertical normal stress. The area under the $-\Delta\sigma_{zz}$ curves is also equal to the ΔGPE* (e.g., Eq. 31). The expression shown in the middle panel, represents the area of the light gray triangle. This is the simplified expression for the trench pull force (e.g. Eq. 34). The concept of a compensation level implies that differences in $\Delta\sigma_{zz}$ have to equilibrate exactly. When the lithostatic approximation is used for stress state beneath the trench (shown in red), there is no equilibration of the vertical normal stress. The right hand panel shows the cumulative ΔGPE*, as a function of depth. All of the black lines converge to the same value, because they are, respectively based on density distributions ($\rho(z)$, $\rho^*(z)$) , which have the same vertical center of mass. In the lithostatic approximation, the ΔGPE* is unbounded.

Appendix A Distribution of vertical shear stress

In deriving the vertical distribution of shear stress, the assumptions are a uniform 2D plate of thickness h, which undergoes plane bending, with zero shear stress on the upper and lower edges. We retain the same coordinate convention (positive down, to the right); we use the primed coordinate system, which is relative to the plate. here, the origin of z' is the center of the plate. Neglecting any in-plane stress resultant, the balance of moments and vertical forces, for a 2D beam/plate equation are expressed as:

$$\frac{dM}{dx} = V(x), \; \frac{dV}{dx} = -f(x) \tag{A1}$$

The normal stress $\sigma_{xx}(z)$ due to bending is:

$$\sigma_{xx}(x, z') = -\frac{M(x) \cdot z'}{I} \tag{A2}$$

where I is the (2D) moment of the area. From Eq. A1, the horizontal gradient of normal stress is:

$$\frac{\partial \sigma_{xx}(x, z')}{\partial x} = -\frac{z' \cdot V(x)}{I} \tag{A3}$$

For the horizontal direction, the stress equilibrium equation is:

$$\frac{\partial \sigma_{xx}}{\partial x} + \frac{\partial \sigma_{zx}}{\partial z'} = 0 \tag{A4}$$

meaning:

$$\frac{\partial \tau_{xz}}{\partial z} = \frac{z' \cdot V(x)}{I} \tag{A5}$$

Integrating with respect to z':

$$\tau_{xz}(x, z') = \int \frac{z' \cdot V(x)}{I} \, dz = \frac{V(x)}{I} \left(\frac{z'^2}{2} \right) + C(x) \tag{A6}$$

Given $\tau_{xz}(x, \pm\frac{h}{2}) = 0$, we can solve for $C(x)$. Substituting $C(x)$ back, we get:

$$\tau_{xz}(x, z') = \frac{V(x)}{I} \left(\frac{z^2}{2} - \frac{h^2}{8} \right) \tag{A7}$$

There are few brief points to note. The maximum value of the vertical shear stress occurs at the center of the plate (or more generally, at the neutral plane), where the horizontal stress is zero. Across the plate, the principal stresses rotate: they are only truly vertically aligned (Andersonian) at the free surface. At the center of the plate, the principal stresses are oriented at 45° from the horizontal: the differential stress is not zero at the middle of the plate, although the quantity σ_{xx} is. For the lithosphere, where gravitational forces obviously contribute to the mean stress, it would be τ_{xx}, or $\Delta\sigma_{xx}$ that are zero at the neutral plane.

Appendix B ΔGPE* as a difference in center of mass

In the manuscript, the ΔGPE* between an isostatic reference column, and a deflected column, is given by:

$$\Delta \text{GPE}^* = g \int_{z_0}^{z_c} \left(\Delta\rho(z) + \Delta\rho^*(z) \right) (z_c - z) dz \tag{B1}$$

From Eq. 15, we know that total integral (mass anomaly) of each density distribution is equal:

$$M = \int_{z_0}^{z_c} \Delta\rho(z)\, dz = \int_{z_0}^{z_c} \Delta\rho^*(z) = (\rho_m - \rho_w) w(x) \tag{B2}$$

where $w(x)$ is the deflection. The difference in the center of mass of each of these distributions (around z_c) can be written as:

$$\begin{aligned} \Delta z_{\text{cm}} &= \frac{1}{M} \int_{z_0}^{z_c} \left(\Delta\rho(z)(z_c - z) \right) dz \\ &- \\ &- \frac{1}{M} \int_{z_0}^{z_c} \left(\Delta\rho^*(z)(z_c - z) \right) dz \end{aligned} \tag{B3}$$

the negative sign on the last line reflects the fact that $\Delta\rho^*(z)$ is a negative quantity, and we wish to define a positive center of mass. Which means we can write Eq. B1 as:

$$\Delta \text{GPE}^* = g M \Delta z_{\text{cm}} \tag{B4}$$

The center of mass of $\Delta\rho(z)$ is given by $z_I - \frac{1}{2} w_T$. Based on the models and assumptions developed in this paper, the center of mass of $\rho^*(z)$ occurs at $z_I + w + \frac{1}{2} z'_m$. The difference is $\frac{1}{2}(w + z'_m)$, as in Eq. 33.

This relationship also allows us to examine the approximation we used in neglecting the crust. Because we neglected the crust, and instead treated the entire column of lithosphere as having background mantle density, we introduced an error in the distribution of $\Delta\rho$. We overestimated the $\Delta\rho$ in the section of lithosphere between z_I and w_T, because we took the density difference as $\rho_m - \rho_m$, whereas the actual density difference is $\rho_m - \rho_c$ (assuming the moho depth (z'_m) is greater than w_T, which is usually correct). This overestimate is balanced by an equal underestimate between the depths $z_I + z'_m$ and $z_I + z'_m + w_T$, where the isostatic column contains mantle rock and the deflected column contains crust. The error in the GPE* can be estimated from Eq. B4, and is $\approx 0.04\ \text{TN}\,\text{m}^{-1}$.

Open Research Section

This manuscript does not contain any new data.

Acknowledgments

This work would not have been possible without support of my partner. I would also like to acknowledge the support of Pete Betts, Sara-Polanco, Rebecca Farrington and Mark Quigley.

References

Becker, T. W., & O'Connell, R. J. (2001). Predicting plate velocities with mantle circulation models. *Geochemistry, Geophysics, Geosystems*, *2*(12).

Bercovici, D., Tackley, P., & Ricard, Y. (2015). 7.07-the generation of plate tectonics from mantle dynamics. *Treatise on Geophysics. Elsevier, Oxford*, 271–318.

Bessat, A., Duretz, T., Hetényi, G., Pilet, S., & Schmalholz, S. M. (2020). Stress and deformation mechanisms at a subduction zone: insights from 2-d thermo-mechanical numerical modelling. *Geophysical Journal International*, *221*(3), 1605–1625.

Bird, P. (1998). Testing hypotheses on plate-driving mechanisms with global lithosphere models including topography, thermal structure, and faults. *Journal of Geophysical Research: Solid Earth*, *103*(B5), 10115–10129.

Bird, P., Liu, Z., & Rucker, W. K. (2008). Stresses that drive the plates from below: Definitions, computational path, model optimization, and error analysis. *Journal of Geophysical Research: Solid Earth*, *113*(B11).

Caldwell, J., Haxby, W., Karig, D. E., & Turcotte, D. (1976). On the applicability of a universal elastic trench profile. *Earth and Planetary Science Letters*, *31*(2), 239–246.

Capitanio, F. A., Morra, G., & Goes, S. (2009). Dynamics of plate bending at the trench and slab-plate coupling. *Geochemistry, Geophysics, Geosystems*, *10*(4).

Capitanio, F. A., Stegman, D. R., Moresi, L.-N., & Sharples, W. (2010). Upper plate controls on deep subduction, trench migrations and deformations at convergent margins. *Tectonophysics*, *483*(1-2), 80–92.

Chapple, W. M., & Forsyth, D. W. (1979). Earthquakes and bending of plates at trenches. *Journal of Geophysical Research: Solid Earth*, *84*(B12), 6729–6749.

Chen, Y.-W., Colli, L., Bird, D. E., Wu, J., & Zhu, H. (2021). Caribbean plate tilted and actively dragged eastwards by low-viscosity asthenospheric flow. *Nature Communications*, *12*(1), 1603.

Clennett, E. J., Holt, A. F., Tetley, M. G., Becker, T. W., & Faccenna, C. (2023). Assessing plate reconstruction models using plate driving force consistency tests. *Scientific reports*, *13*(1), 10191.

Coblentz, D., van Wijk, J., Richardson, R. M., Sandiford, M., Foulger, G., Lustrino, M., & King, S. (2015). The upper mantle geoid: Implications for continental structure and the intraplate stress field. *Geological Society of America Special Papers*, *514*, 197–214.

Conrad, C. P., & Lithgow-Bertelloni, C. (2002). How mantle slabs drive plate tectonics. *Science*, *298*(5591), 207–209.

Copley, A., Avouac, J.-P., & Royer, J.-Y. (2010). India-asia collision and the cenozoic slowdown of the indian plate: Implications for the forces driving plate motions. *Journal of Geophysical Research: Solid Earth*, *115*(B3).

Craig, T., Copley, A., & Jackson, J. (2014). A reassessment of outer-rise seismicity and its implications for the mechanics of oceanic lithosphere. *Geophysical Journal International*, *197*(1), 63–89.

Davies, G. F. (1983). Subduction zone stresses: constraints from mechanics and from topographic and geoid anomalies. *Tectonophysics*, *99*(2-4), 85–98.

Drucker, D. (1956). The effect of shear on the plastic bending of beams.

Elasasser, W. M. (1969). Convection and stress propagation in the upper mantle. *The application of modern physics to the Earth and planetary interiors*, 223–246.

England, P., & Molnar, P. (2022). Changes in plate motions caused by increases in gravitational potential energy of mountain belts. *Geochemistry, Geophysics, Geosystems*, *23*(10), e2022GC010389.

Fleitout, L., & Froidevaux, C. (1983). Tectonic stresses in the lithosphere. *Tectonics*, *2*(3), 315–324.

Forsyth, D., & Uyeda, S. (1975). On the relative importance of the driving forces of plate motion. *Geophysical Journal International*, *43*(1), 163–200.

Garcia, E. S. M., Sandwell, D. T., & Bassett, D. (2019). Outer trench slope flexure and faulting at pacific basin subduction zones. *Geophysical Journal International*, *218*(1), 708–728.

Goetze, C., & Evans, B. (1979). Stress and temperature in the bending lithosphere as constrained by experimental rock mechanics. *Geophysical Journal International*, *59*(3), 463–478.

Goodier, J. N., & Timoshenko, S. (1970). *Theory of elasticity*. McGraw-Hill.

Grellet, C., & Dubois, J. (1982). The depth of trenches as a function of the subduction rate and age of the lithosphere. *Tectonophysics*, *82*(1-2), 45–56.

Hager, B. H., & O'Connell, R. J. (1981). A simple global model of plate dynamics and mantle convection. *Journal of Geophysical Research: Solid Earth*, *86*(B6), 4843–4867.

Hirth, G., & Kohlstedt, D. (2003). Rheology of the upper mantle and the mantle wedge: A view from the experimentalists. *Geophysical monograph-american geophysical union*, *138*, 83–106.

Horne, M. R. (1951). The plastic theory of bending of mild steel beams with particular reference to the effect of shear forces. *Proceedings of the Royal Society of London. Series A. Mathematical and Physical Sciences*, *207*(1089), 216–228.

Hunter, J., & Watts, A. (2016). Gravity anomalies, flexure and mantle rheology seaward of circum-pacific trenches. *Geophysical Journal International*, *207*(1), 288–316.

Isacks, B., & Molnar, P. (1971). Distribution of stresses in the descending lithosphere from a global survey of focal-mechanism solutions of mantle earthquakes. *Reviews of Geophysics*, *9*(1), 103–174.

Lemenkova, P. (2019). Geomorphological modelling and mapping of the peru-chile trench by gmt. *Polish Cartographical Review*, *51*(4), 181–194.

Lister, C. R. (1975). Gravitational drive on oceanic plates caused by thermal contraction. *Nature*, *257*(5528), 663–665.

McAdoo, D. C., Caldwell, J. G., & Turcotte, D. L. (1978, 07). On the elastic-perfectly plastic bending of the lithosphere under generalized loading with application to the Kuril Trench. *Geophysical Journal International*, *54*(1), 11-26. Retrieved from `https://doi.org/10.1111/j.1365-246X.1978.tb06753.x` doi: 10.1111/j.1365-246X.1978.tb06753.x

McNutt, M. K., & Menard, H. (1982). Constraints on yield strength in the oceanic lithosphere derived from observations of flexure. *Geophysical Journal International*, *71*(2), 363–394.

Melosh, J. (1977). Shear stress on the base of a lithospheric plate. *Stress in the Earth*, 429–439.

Molnar, P., & Bendick, R. (2019). Seismic moments of intermediate-depth earthquakes beneath the hindu kush: Active stretching of a blob of sinking thickened mantle lithosphere? *Tectonics*, *38*(5), 1651–1665.

Parsons, B., & Molnar, P. (1976). The origin of outer topographic rises associated with trenches. *Geophysical Journal International*, *45*(3), 707–712.

Richardson, R. M., Solomon, S. C., & Sleep, N. H. (1979). Tectonic stress in the plates. *Reviews of Geophysics*, *17*(5), 981–1019.

Richter, F., McKenzie, D., et al. (1977). Simple plate models of mantle convection. *Journal of Geophysics*, *44*(1), 441–471.

Sandiford, D., Betts, P., Whittaker, J., & Moresi, L. (2024). A push in the right direction: Exploring the role of zealandia collision in eocene pacific-australia plate motion changes. *Tectonics*, *43*(3), e2023TC007958.

Sandiford, D., & Craig, T. J. (2023). Plate bending earthquakes and the strength distribution of the lithosphere. *Geophysical Journal International*, *235*(1), 488–508.

Sandiford, M., Coblentz, D., & Schellart, W. P. (2005). Evaluating slab-plate coupling in the indo-australian plate. *Geology*, *33*(2), 113–116.

Saxena, A., Dannberg, J., Gassmöller, R., Fraters, M., Heister, T., & Styron, R. (2023). High-resolution mantle flow models reveal importance of plate boundary geometry and slab pull forces on generating tectonic plate motions. *Journal of Geophysical Research: Solid Earth*, *128*(8), e2022JB025877.

Schellart, W. (2004). Quantifying the net slab pull force as a driving mechanism for plate tectonics. *Geophysical research letters*, *31*(7).

Spence, W. (1987). Slab pull and the seismotectonics of subducting lithosphere. *Reviews of Geophysics*, *25*(1), 55–69.

Tanimoto, B. (1957). Stress analysis of a gravitating simply-supported beam. , *7*, 15–20.

Turcotte, D. L., McAdoo, D., & Caldwell, J. (1978). An elastic-perfectly plastic analysis of the bending of the lithosphere at a trench. *Tectonophysics*, *47*(3-4), 193–205.

Turcotte, D. L., & Schubert, G. (2002). *Geodynamics*. Cambridge university press.

van Summeren, J., Conrad, C. P., & Lithgow-Bertelloni, C. (2012). The importance of slab pull and a global asthenosphere to plate motions. *Geochemistry, Geophysics, Geosystems*, *13*(2).

Wiens, D. A., & Stein, S. (1985). Implications of oceanic intraplate seismicity for plate stresses, driving forces and rheology. *Tectonophysics*, *116*(1-2), 143–162.

Zhang, F., Lin, J., & Zhan, W. (2014). Variations in oceanic plate bending along the mariana trench. *Earth and Planetary Science Letters*, *401*, 206–214.